Journal of Structural Geology, Vol. 15, No. 6, pp. 693 to 706, 1993
Printed in Great Britain

0191-8141/93 $06.00 + 0.00

Structural and strain analyses of the middle part of the Talassian Alatau ridge (Middle Asia, Kirgizstan)

ANDREW K. KHUDOLEY

All Union Geological Research Institute (VSEGEI), 199026, St. Petersburg, Sredny Prospect, 74, Russian Federation

(*Received* 18 *June* 1991; *accepted in revised form* 24 *July* 1992)

Abstract—The middle part of the Talassian Alatau ridge is composed of Upper Precambrian–Lower Paleozoic greenschists (the Usunakhmatian sheet), which were overthrust on unmetamorphosed rocks of nearly the same age (the Talassian and Kumishtagian sheets). Three phases of deformation can be recognized in the Usunakhmatian sheet, the most intensive of which was the Late Silurian–Early Devonian D_2 deformation.

In the Usunakhmatian sheet, the axis of maximum extension is subhorizontal and parallel to F_2 fold axes. R_{xz} varies from 2.4 to 7.5 and k from 0.03 to 1.75. Flattening is widespread, but the strain of many samples is nearly plane strain. In the Talassian sheet, R_{xz} varies from less than 1.8. to 4.4 and k from 0 to 0.35. R_{xz} and k values increase near large faults. R_{xz} values determined by quartz and chert grains were found to be linearly related. A three-stage strain history is related to D_2 deformation. The earliest was simple shear parallel to the axial surfaces of folds. Following this, the fold and thrust system was transformed by pure shear with an orogen-parallel axis of extension. Some minor increments of strain are locally represented by pressure shadows around pyrite crystals.

INTRODUCTION

THE Talassian Alatau mountain ridge is located in the northwestern part of Kirgizia in Middle Asia. The main tectonic and stratigraphic features of the region are shown in Fig. 1. The Talaso–Ferganian Fault (TFF) divides the ridge in two parts with different tectonic histories. The central and northeastern parts of the ridge belong to the Caledonides of the Northern Tien-Shan and the southwestern part to the Hercynides of the central Tien-Shan (Kiselev & Korolev 1981, Korolev *et al.* 1983, Afonichev & Vlasov 1984).

There are three large tectonic sheets in the Caledonian part of the region (Figs. 1c & d). The Kumishtagian sheet is composed of Proterozoic (Vendian)–Middle Ordovician carbonate platform and tidal sediments (Pomazkov *et al.* 1972, Kiselev & Korolev 1981, Becker *et al.* 1988). The Talassian sheet consists mostly of submarine fan terrigeneous and shelf carbonate–terrigeneous sediments. Limited to the upper part are lagoonal red shales. The age of rocks of this sheet is generally believed to be Late Precambrian (Late Riphean–Vendian) (Pomazkov *et al.* 1972, Goncharov 1979, Kiselev & Korolev 1981, Becker *et al.* 1988), but the upper part of the sequence may be as young as Early Paleozoic (Khudoley & Semiletkin in press). In the northeast of the Talassian Alatau rocks are slightly altered and a spaced cleavage is present only in shales. To the southeast sandstones become cleaved, but sedimentary structures are still readily recognizable. The Usunakhmatian sheet contains the same formations as the Talassian one but has been metamorphosed to greenschist facies and primary sedimentary structures can not often be distinguished. According to Goncharov (1979) and Frolova (1982) structural–metamorphic zonation is subparallel to the TFF.

The purpose of this paper is to study the nature of deformation and strain of the Usunakhmatian sheet. This tectonic unit is of particular interest because of its intense deformation and contiguity to the TFF—one of the largest lineament of Middle Asia. The TFF is usually considered to be a dextral strike-slip fault with a displacement up to 200 km (Burtman 1964, Suvorov 1968), though the magnitude of the net slip is controversial (Beloussov 1975, p. 37). Some deformation characteristics of the Talassian sheet are given for comparison.

REGIONAL STRUCTURE

The Usunakhmatian sheet is bounded on the southwest by the TFF and on the northeast by the Central Talassian Thrust (CTT) (Fig. 1c). The CTT is an easily identified fault in the eastern and central parts of the region, where greenschists are thrusted onto unmetamorphosed rocks of the Talassian and Kumishtagian sheets. The thrust surface is locally accompanied by thick zones of brecciation and mylonitization. In the western part, the single thrust breaks up into a series of parallel faults (Goncharov 1979, Frolova 1982) and the boundary between the Usunakhmatian and Talassian sheets is not distinct.

The main phases of the deformation of the Usunakhmatian sheet and their respective orientation characteristics are shown in Figs. 2 and 3. D_1 structures are not widespread. In the western part of the sheet they are represented by small open and closed F_1 folds, the axial planes of which change orientation on the limbs of later folds (Fig. 3a, F_1). F_1 axial planes are cut at a considerable angle by S_2 cleavage in the eastern part of the region (Becker 1987).

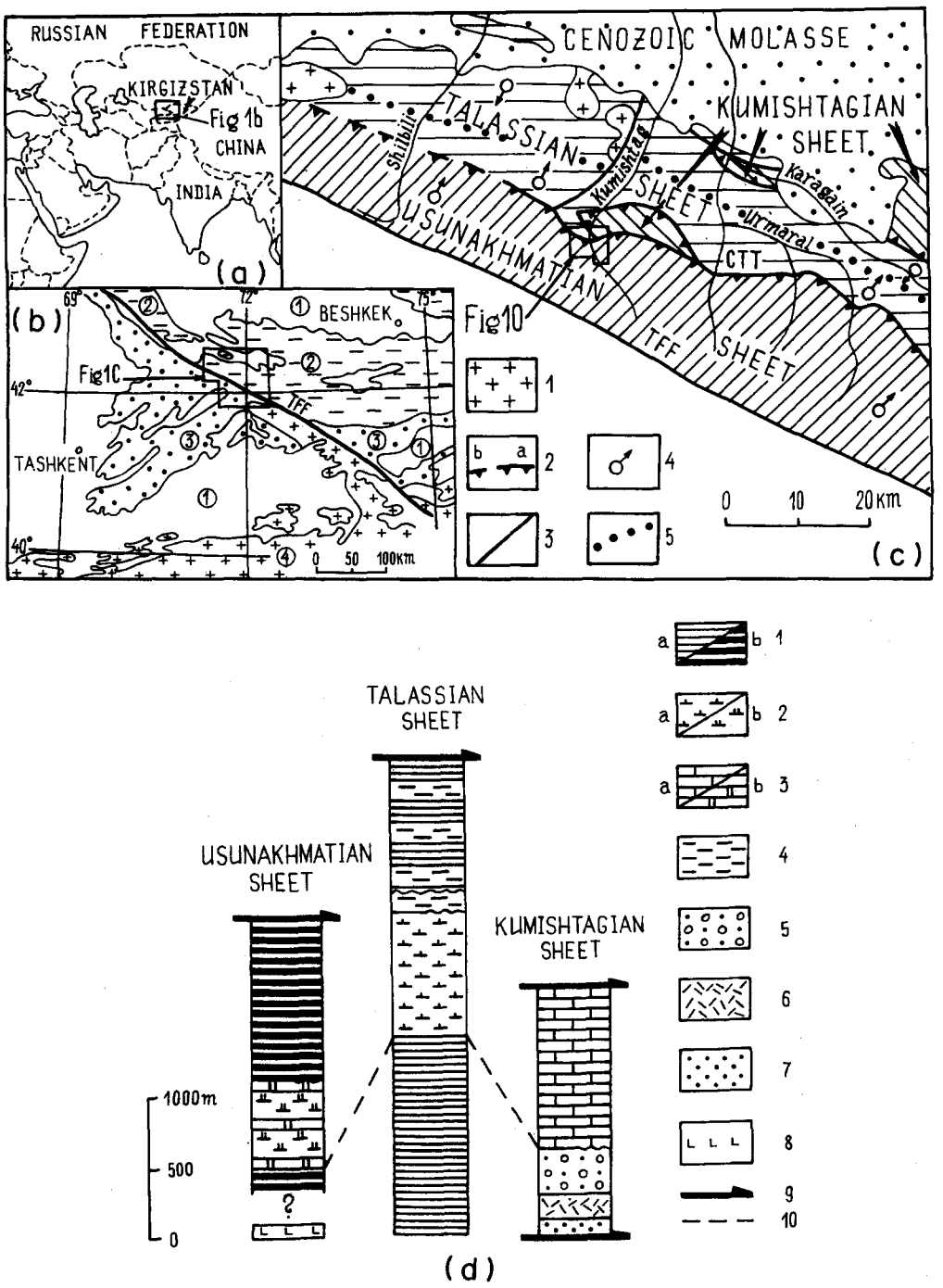

Fig. 1. Main tectonic and stratigraphic features of the Talassian Alatau ridge. (a) Geographical setting. (b) Regional tectonic map, symplified from Afonichev & Vlasov (1984). 1—Mesozoic and Cenozoic orogenic and platform cover sediments; 2-4—fold-thrust systems: 2—Northern Tien-Shan, Caledonides; 3—Middle Tien-Shan, Hercynides; 4—Southern Tien-Shan, Hercynides; TFF—Talaso-Ferganian Fault. (c) Tectonic map of Talassian Alatau ridge (Khudoley & Semiletkin in press). 1—granites; 2—boundaries between sheets: single thrust (a) and series of parallel thrusts (b); 3—strike-slip faults; 4—direction of structural vergence; 5—boundary between regions with opposite vergence. (d) Stratigraphic columns of the Talassian Alatau sheets. Thicknesses not corrected for strain. 1—terrigeneous rhythmites unmetamorphosed (a) and metamorphosed (b); 2—terrigeneous–calcareous rhythmites unmetamorphosed (a) and metamorphosed (b); 3—massive carbonates unmetamorphosed (a) and metamorphosed (b); 4—mudstones; 5—diamictites; 6—acid tuffs and minor cherts; 7—sandstones; 8—metamorphosed basalts; 9—thrusts; 10—boundary between Precambrian and Cambrian (according Khudoley & Semiletkin in press).

The dominant structure in the region was formed during D_2 penetrative deformation. It is characterized by a strong parallelism of the F_2 axial planes, S_2 cleavage (Fig. 3a, S_0 and S_2) and imbricate thrusts. The latter form a leading imbricate fan (Boyer & Elliott 1982). F_2 folds are cylindrical or subcylindrical and overturned to the north-northeast (Fig. 3a, S_0 and F_2). Reversals in fold axis plunge (Fig. 3a, S_0) are due to primary hinge curvature, not later refolding. Small F_2 folds are tight to isoclinal, and large F_2 folds are tight to close. The shape of folds depends on the lithology of beds. Folds in pelitic schists have class 2 and 3 geometry (Ramsay 1967,

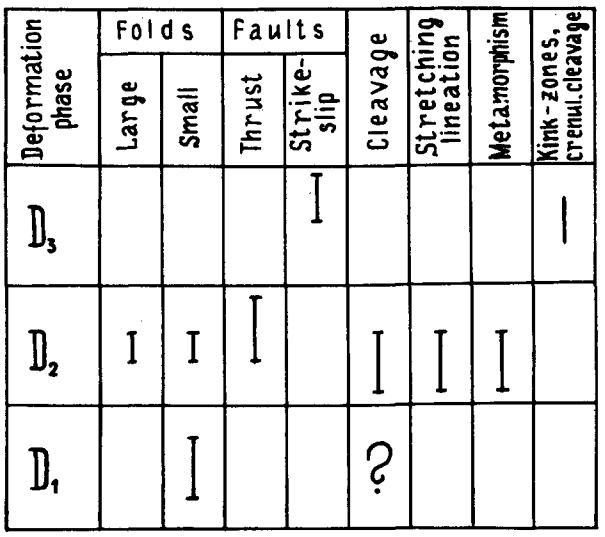

Fig. 2. History of the development of the Unsunakhmatian sheet structural elements.

p. 365) whereas folds in psammitic schists and metacarbonates have class 1C and 2 geometry. S_2 cleavage is widespread; continuous cleavage (Borradaile *et al.* 1982) dominates, with spaced cleavage (smooth and rough) in less altered psammitic schists. There are two types of lineation: cleavage–bedding intersections and stretching lineations, the latter expressed by a preferred orientation of the long axes of detrital and new grains. Both types of lineation are parallel to fold axes (Fig. 3a, S_0 and L_2). Dips of F_2 axial planes, S_2 cleavage and imbricated thrusts increases from 40° to 45° at the CTT to subvertical at the TFF.

The development of the various D_2 structures was not coeval (Fig. 2). The formation of cleavage and metamorphism slightly pre-dates folding (Goncharov 1979, Frolova 1982) whereas the formation of imbricate thrusts continued for some time after folding (Becker 1987). As the metasedimentary rocks of the Usunakhmatian sheet are overthrusted on the carbonates of Cambrian–Middle Ordovician, the D_2 deformation could not have taken place earlier than the end of Middle Ordovician. Thrust–fold structures are cut by polyphase intrusions of leucocratic granites analogous with the Caledonian granites of the Northern Tien-Shan. Two sets of concordant U–Pb ages are interpreted as the age of crystallization of older and younger parts and show 710 ± 25 and about 400 Ma, respectively (Kiselev *et al.* 1986). The latter characterizes the upper limit for the age of deformation.

D_3 structures are only locally developed. They are represented by kink zones, crenulation cleavage (Fig. 3a, F_3) and small strike-slip faults, approximately parallel to the kink zones. Their oblique relations with the TFF (Fig. 4) show that the origin of these structures is connected with dextral strike-slip displacements along the TFF (Beloussov 1985, p. 174, Sylvester 1988). The dextral strike-slip displacements along the TFF began not earlier than in Late Paleozoic (Burtman 1962); the same age have D_3 structures. D_3 deformation led to local reorientation of D_2 structures from parallel to the TFF up to oblique.

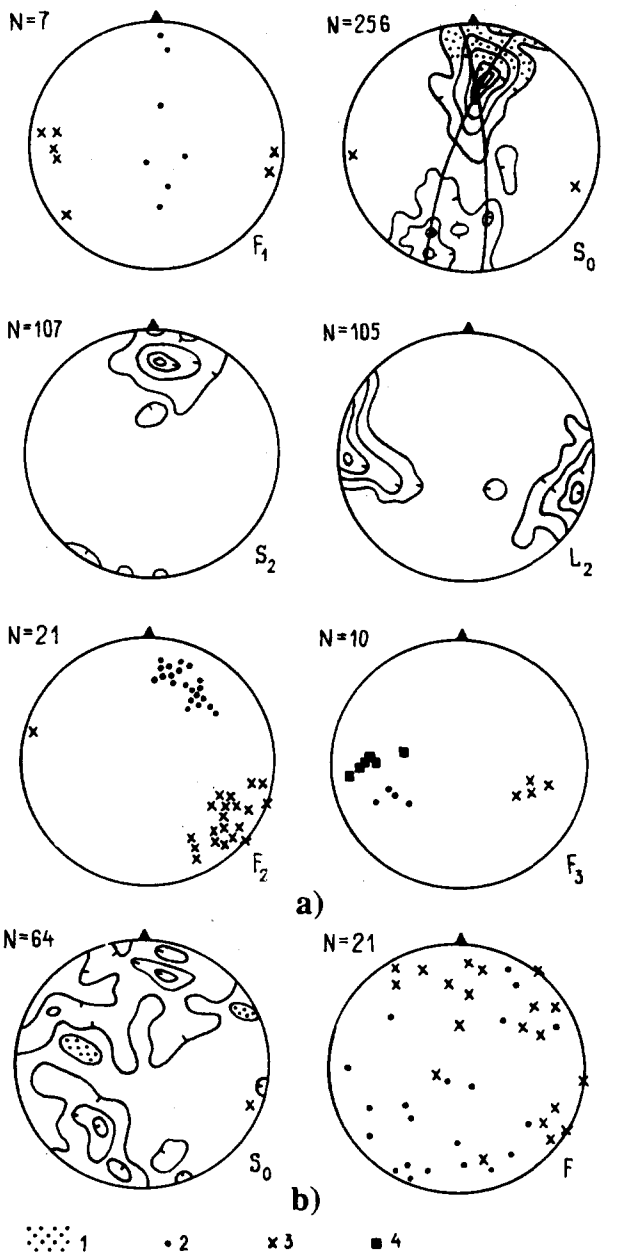

Fig. 3. Orientation characteristics of (a) the Usunakhmatian sheet and (b) the south part of the Talassian sheet. Structures of the Talassian sheet are not separated onto different deformation phases. 1—overturned bedding is predominant; 2—poles to axial planes of folds; 3—fold axes; 4—poles to kink zones. Contours: (a) S_0 1–3–6–10–14%; S_2 1–10–25–40–50%; L_2 1–5–10–20%. (b) S_0 2–5–8%. Hactures show direction of increasing concentration.

The detailed description of structural geology of the Talassian and Kumishtagian sheets lies beyond the scope of this paper. Here it is noted that early deformation phases within them had SSW vergence and predate the D_2 deformation of the Usunakhmatian sheet (Khudoley & Semiletkin in press). During these deformations the Kumishtagian and, partly, Talassian sheets were overthrusted on the Usunakhmatian sheet. The two latter deformation phases in the Talassian and Kumishtagian sheets coincide with D_2 and D_3 stages and are the result of deformation processes in the Usunakhmatian sheet. Some orientation data from the Talassian sheet near the CTT are shown in Fig. 3(b).

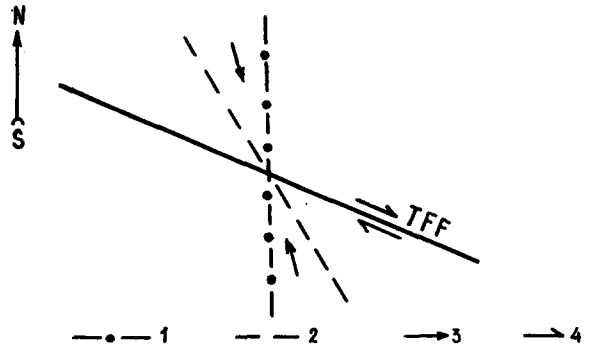

Fig. 4. Relationship between D_3 structural elements of the Usunakhmatian sheet and the TFF (dextral strike-slip fault). 1—strike of kink zones; 2—strike of crenulation cleavage; 3—direction of stress action; 4—direction of movements.

DESCRIPTION OF SAMPLES AND METHODS OF STRAIN ANALYSIS

The most widespread strain markers in the Usunakhmatian sheet are detrital grains in terrigeneous schists. Clasts of gravel size (15 samples) were studied directly in the field whereas 12 pairs of oriented thin sections, from psammitic schists, were examined in the laboratory. In all cases the observations were carried out in the XZ plane and in one more principal plane (usually YZ, rarely XY). The axial ratio in the third plane was estimated by the equation $R_{xz} = R_{xy}R_{yz}$ (Ramsay & Huber 1983, p. 170).

Typical samples of terrigeneous schists are shown in Fig. 5, which are dominated by quartz and chert fragments. The former are widespread and the latter are common only in conglomeratic schists. There are grains of altered feldspars, biotites, granitoids and schists in small quantities. Grains are poorly sorted and matrix-supported. Pressure solution seams are clearly seen in thin section (Fig. 5b).

Quartz and chert grains have been studied separately. The R_f/ϕ method (Ramsay 1967, pp. 209–211) has been applied to all the samples. The calculations were carried out on the hyperbolic net of De Paor (1988). Eighteen measurements of strain were made with the use of the Lisle nets (Lisle 1985, pp. 28–77) and seven samples were studied with the Fry method (Fry 1979, Ramsay & Huber 1983). The harmonic mean (Lisle 1977, 1985, Ramsay & Huber 1983, pp. 111–113) was calculated for all the samples with $R_s > 2.0$. Between 20 and 70 grains per plane were counted when the R_f/ϕ or harmonic mean methods were used and 200–425 grains were counted for the usage of the Fry (1979) method (Fig. 6). Altogether in the Usunakhmatian sheet strain was determined at 31 localities.

Strain analysis of the Talassian sheet was based mostly on reduction spots in red shales (Fig. 5c). It is assumed that the reduction spots were initially spherical (Ramsay & Huber 1983, p. 174, Uemura & Mizutani 1984, p. 173) and their final shape represents the total strain ellipsoid. A qualitative estimate of strain is also provided by the occurrence of pencil cleavage which has been shown to occur at small intensities of strain (Reks & Gray 1982). In total in the Talassian sheet (near the CTT) strain was determined in 12 localities.

RESULTS

Strain ellipsoid orientations

The orientation data discussed below were obtained by calculations on the hyperbolic net (De Paor 1988) and are shown in Fig. 7. Measurements were made with reference to cleavage planes, which are easily visible at every outcrop. Considering absolute values of $\Delta\phi$ only, which implies a symmetrical shape of the orientation distribution and allows only the right side of distribution with doubled values to be considered. The best approximation to the distribution in Fig. 7(a) is a Laplace one, but this type of distribution fits poorly to the data in Fig. 7(b). There is no reason to suppose that distributions in Figs. 7(a) & (b) have a different nature and, therefore, both distributions should be of the same type. With this consideration, the best approximation is found to be a normal distribution with dispersion $\sigma^2 = 1.35$ (Fig. 7a) and $\sigma^2 = 2.22$ (Fig. 7b).

The above results might have the following interpretation. Probability that $\Delta\phi < 3°$ (Fig. 7a) is high and equals to $P\{0 < \Delta\phi < 3°\} = 2\{\Phi(0.86) - \Phi(0)\} = 0.61$ (coefficient 2 is the result of doubling) and implies that, within error limits, the X axis lies in the plane of cleavage and, according to field observations, is subhorizontal. This agrees well with data indicating parallelism of the stretching lineation, cleavage–bedding intersection lineation and fold axes (see Fig. 3a, S_0, L_0, and Fig. 5a). For the distribution in Fig. 7(b) probabilities of $\Delta\phi < 3°$, $3° < \Delta\phi < 6°$ and $\Delta\phi < 6°$ are equal to 0.50, 0.32 and 0.18, respectively. These data show that probability of $3° < \Delta\phi < 6°$ is relatively high, although probability of $\Delta\phi < 3°$ is higher. From this we conclude that the normal distribution in Fig. 7(b) neither supports nor rejects the idea of strict parallelism of the XY plane of the strain ellipsoid and cleavage planes (Ramsay 1967, p. 180, Ramsay & Huber 1983, p. 181, Uemura & Mitzutani 1984, p. 175, Beloussov 1985, p. 158) and of some minor angle being present between these planes (Ghosh 1982, Treagus 1988). This angle is too small to affect significantly the accuracy of calculations and for simplicity, the XY plane is considered to be parallel to the cleavage plane. Obviously, the Z axis is normal or subnormal to the cleavage plane.

Comparison of results obtained by different methods and markers

Different methods of strain analysis of elliptical objects generally give similar axial ratios (Table 1) and their results are summarized in Fig. 8. The difference between the techniques of Lisle (1985) and De Paor (1988) is within error limits and not more than the difference between others R_f/ϕ techniques (Paterson 1983). Relatively higher values of the harmonic mean

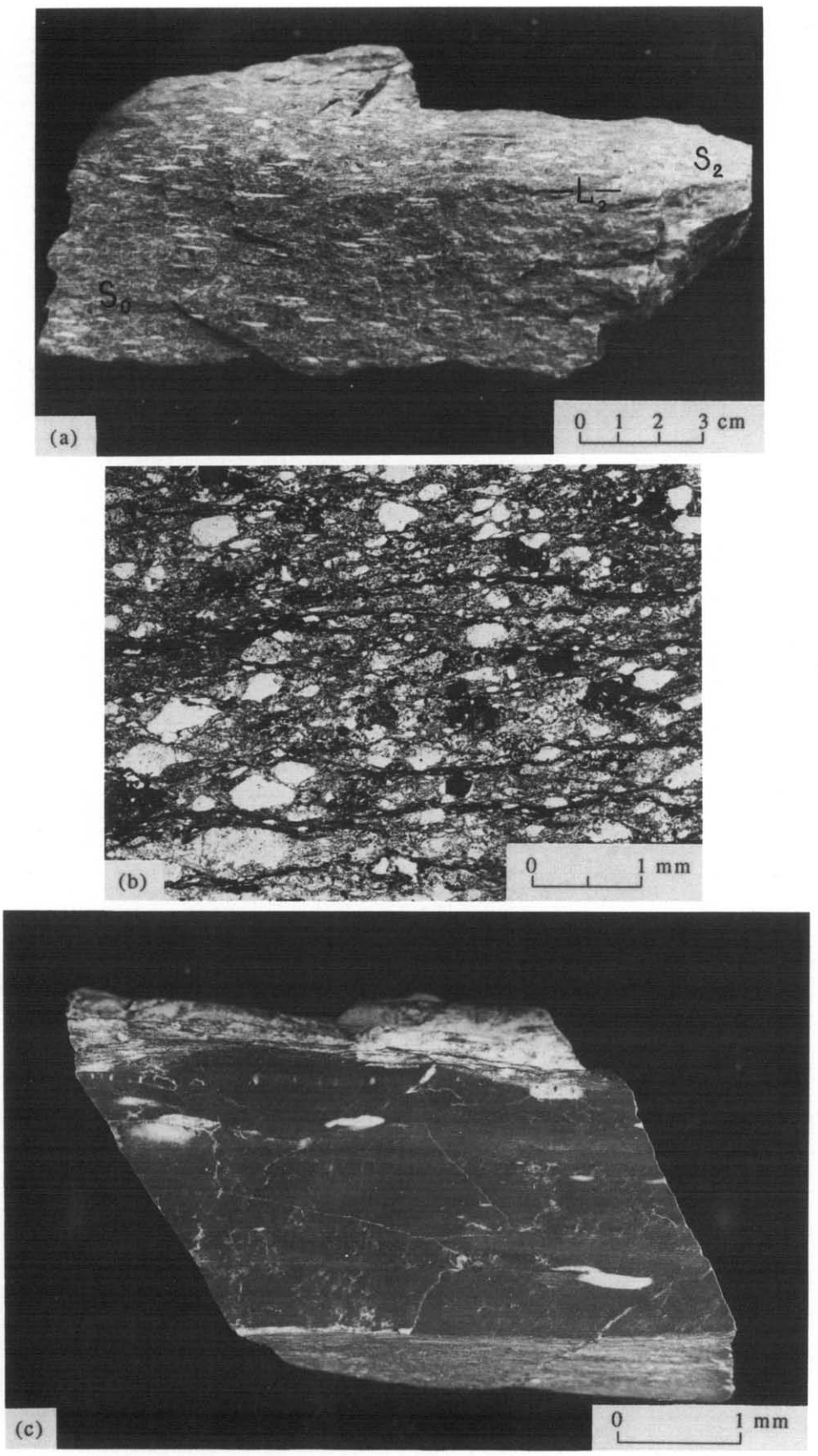

Fig. 5. Typical strain markers. (a) Chert pebbles in pebble–psammitic schists. (b) Quartz grains in psammitic schists, XZ plane. (c) Reduction spots.

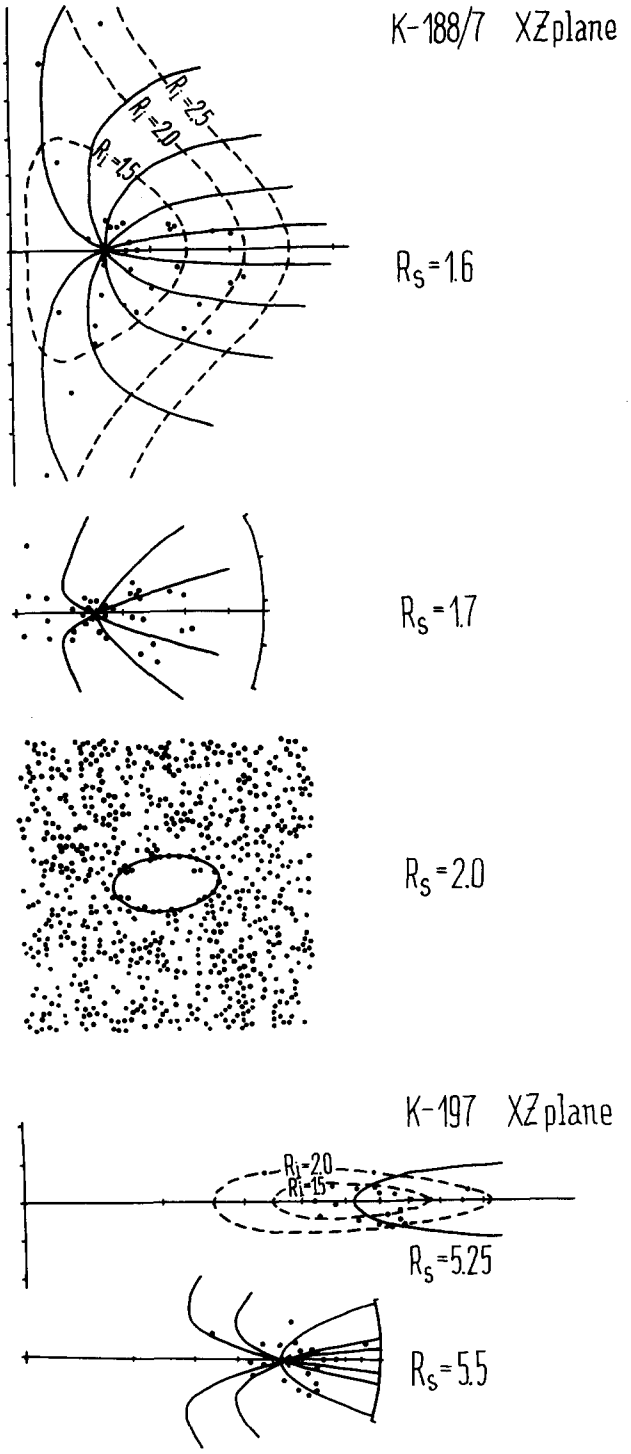

Fig. 6. Two typical examples of determination of strain in sample K-188/7 (*XZ* plane, quartz grains in psammitic schist) by the Fry (1979), Lisle (1985) and De Paor (1988) methods and in sample K-197 (*XZ* plane, chert grains in conglomeratic schist) by the Lisle (1985) and De Paor (1988) methods.

accord with the predictions of Lisle (1977, 1985, p. 18). The Fry method was used to determine strain in thin sections from quartz grains only. These grains were recrystallized and affected by local dissolution and reprecipitation of material (Fig. 5b). According to Dunne *et al.* (1990) the use of the Fry method to recrystallized grains underestimates the true strain. This means, that the R_f/ϕ estimates of strain, being lower than estimates produced by the Fry method (Table 1), lead to considerable underestimation of the true strain. As Onasch (1984, 1986) showed, pressure solution and volume loss distorts the R_f/ϕ method results and leads to reduced R_s values in comparison with homogenous deformation, whereas the Fry method yields predictable results. It is possible that difference between R_s estimations by the Fry and R_f/ϕ methods is due to pressure solution and some volume loss. The De Paor (1988) technique was the method of strain estimation usually applied and only a discussion of its application is given in the text below.

The comparison of axial ratios determined in the same samples on quartz and chert grains shows (Fig. 9) that there is a linear relationship between them:

$$R_{xz(\mathrm{cht})} - 1 = C(R_{xz(\mathrm{qu})} - 1)\,, \qquad (1)$$

where $R_{xz(\mathrm{cht})}$ and $R_{xz(\mathrm{qu})}$ are the axial ratios calculated by the R_f/ϕ method on chert and quartz grains, respectively, the coefficient C equals 3.2.

Regional strain variations

Strain measurements on chert and quartz grains show different results because of viscosity contrasts between them (Table 1, Fig. 8). However, equation (1) allows a comparison of these data. The value of strain obtained by quartz grains was recalculated using equation (1) to estimate the strains of chert grains strain when present in the sample. Axial ratios obtained by recalculations are given in brackets differing from data on chert grains given without brackets (Fig. 10). A knowledge of the values R_{xz} and k make it possible to calculate all other deformation parameters of the strain ellipsoid (Ramsay & Huber 1983, p. 200); for this reason only these parameters are given.

In the Usunakhmatian sheet the values of R_{xz} vary from 7.5 to 2.4 and k from 1.75 to 0.03. In the Talassian sheet R_{xz} ranges from 4.4 to less than 1.8 in the regions of pencil structure development (Khudoley & Semiletkin in press). There is no obvious relationship between R_{xz}, k and fold structures (Fig. 10). For instance, for most of the southern syncline on the left bank of the River Kumishtag (Fig. 10a) the lowest value of R_{xz} (3.6) occurs near the trace of the axial plane, but 2.5 km to the west, near the trace of the same axial plane, R_{xz} increases to 7.5. The relationship with faults seems more definite. Nearing faults k rises and R_{xz} contours are approximately parallel to main thrusts. The increase in R_{xz} and k values is well expressed near the CTT and in the southern part of the area in Fig. 10, relating to the proximity to the TFF.

Similar relationships can be seen in other parts of the region. In the Talassian sheets R_{xz} is not less than 4.0 near the CTT (Fig. 10a). At a distance of about 3 km to the north of the CTT R_{xz} is 2.6–2.8 and at a distance of 4–5 km does not exceed 2.0. k values near the CTT are also higher than at some distance from it (Fig. 10b). In the basin of the River Shilbili (Fig. 1c) the CTT is represented by a series of parallel faults without large

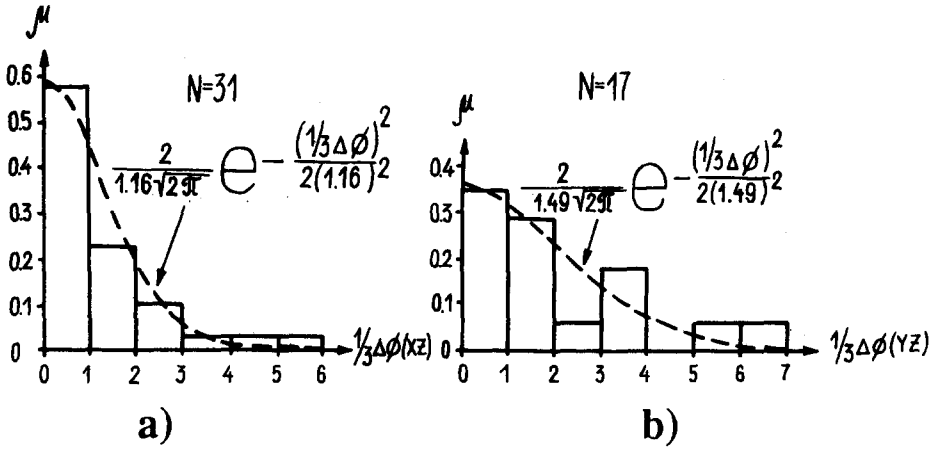

Fig. 7. Histograms of distribution of angles ($\Delta\phi$) between (a) the X axis and the trace of cleavage on the XZ plane and (b) the Y axis and the trace of cleavage on the YZ plane. μ is frequency.

Table 1. The comparison of axial ratios of strain ellipses calculated using various techniques

Chert grains in conglomeratic schists					Quartz grains in psammitic schists				
			R_f/ϕ technique				R_f/ϕ technique		
Field number	Plane	Harmonic mean (H)	De Paor (1988)	Lisle (1985)	Field number	Plane	De Paor (1988)	Lisle (1985)	Fry method
K-188	XZ	6.7	6.2	5.75	K-188/3	XZ	1.9		2.6
K-189	XZ	3.7	3.6			YZ	1.1		1.7
K-197	XZ	5.7	5.5	5.25	K-188/6	XZ	2.1	2.0	2.4
	YZ	3.2	2.9			YZ	1.5	1.3	1.6
K-198	XZ	3.4	3.6	3.4	K-188/7	XZ	1.7	1.6	2.0
K-200	XZ	4.2	4.1	3.9		YZ	1.4	1.35	1.4
K-201 · 9	XZ	3.4	3.3		K-194/5	XZ	1.7		2.4
K-201 · 10		6.2	5.8	5.5		YZ	1.3		1.5
K-218		3.3	3.4		K-195/1	XZ	1.7	1.7	1.8
K-230	XZ	3.7	4.1	3.6		YZ	1.5	1.3	1.5
K-235	XZ	3.0	3.0		K-197/1	XZ	1.9	1.8	2.1
K-239	XZ	4.9	4.9			YZ	1.7	1.5	2.0
	XY	2.4	2.3		K-219	XZ	1.4		1.5
K-2491	XZ	3.6	3.5	3.3		YZ	1.2		1.3
K-249h	XZ	3.8	3.7						
K-253	XZ	3.5	3.0						
K-255	XZ	2.7	2.4	2.4					

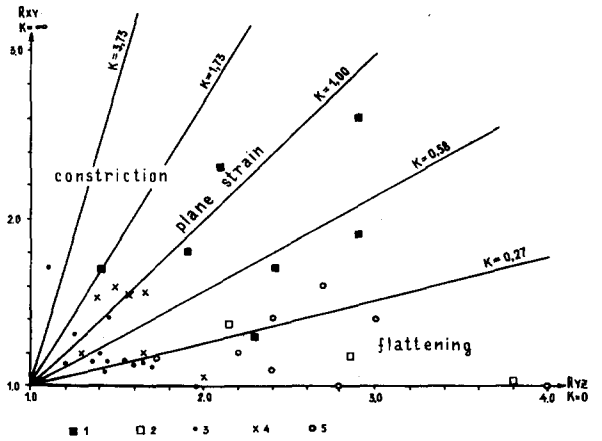

Fig. 8. Flinn plot of principal components of finite strain measured: in the Usunakhmatian sheet (1–4): 1—chert pebbles; 2—chert grains in sandstones; 3—quartz grains (R_f/ϕ method, De Paor 1988 technique); 4–quartz grains (Fry method); in the southern part of the Talassian sheet (5), reduction spots. K is the Flinn parameter.

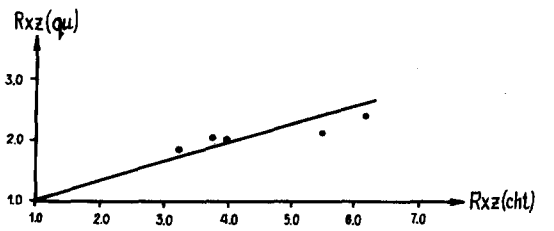

Fig. 9. Relationship between R_{xz} values measured by quartz grains $R_{xz(qu)}$ and chert grains $R_{xz(cht)}$. The straight line corresponds to graph of linear relationship $R_{xz(cht)} - 1 = 3.2\ (R_{xz(qu)} - 1)$.

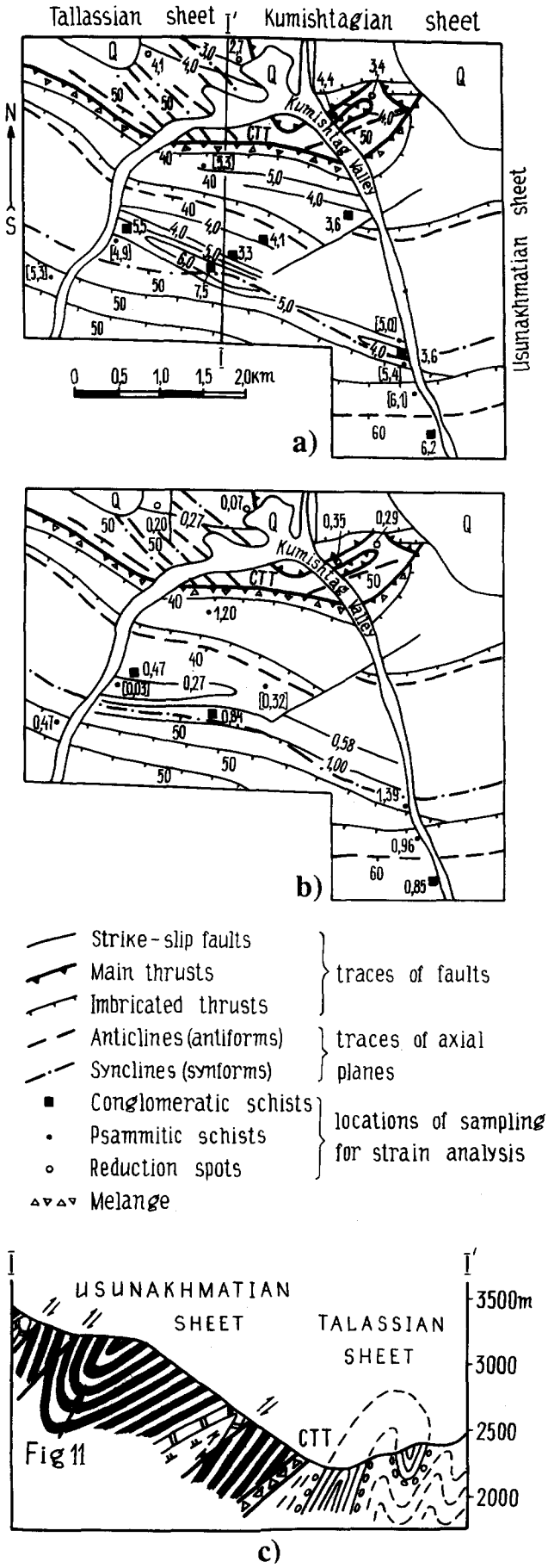

Fig. 10. Strain characteristics of the Usunakhmatian and Talassian sheets. Location of the region is shown in Fig. 1(b). (a) Map of R_{xz} contours; (b) map of k contours; (c) cross-section along the line I–I'. Legend symbols are as in Fig. 1(d).

displacement, and here R_{xz} is 2.4. Going south, R_{xz} increases first to 3.0–5.4 (7–8 km to the north of the TFF) and then to 4.9–6.1 (5 km to the north of the TFF). In the basin of the River Urmaral near the CTT R_{xz} reaches 4.0 in the Talassian sheet and 4.8 in the Usunakhmatian sheet.

Generally, the nearer the main faults (CTT and TFF), the larger B_{xz} and k values. Similar relationships are observed in the Scandinavian Caledonides (Milton & Williams 1981), the Variscian shear zones of the Bohemian Massif (Rajlich 1990), different parts of the Himalayas (Bossart *et al.* 1988, Jain & Anand 1988), the Klamath Mountains (Cashman 1988) the Sierra Nevada, California (Paterson *et al.* 1989, Paterson & Wainger 1991) and the Ballarat Slate Belt of Australia (Gray & Willman 1991).

DISCUSSION

Strain of markers with different viscosity

Equation (1) describing the linear relationship between strain ratios of markers with different viscosity was derived from five samples and needs a verification. Recalculation of R_{xz} data on quartz and pelitic schists pebbles from the Otago Schists, New Zealand (Norris & Bishop 1990, Table 2) supports the use of equation (1) but with C equal to 3.5. For the determination of the nature of the coefficient C the author used the data from Lisle *et al.* (1983, figs. 3 and 5). If the linear equation (1) is true, then (using mean value of R_{xz} for each pair of lithologically different markers) coefficient C is approximately equal to viscosity ratios of markers and the equation (1) may be written as follows:

$$R_{xz(a)} - 1 = \frac{V_b}{V_a}(R_{xz(b)} - 1), \qquad (2)$$

where $R_{xz(a)}$ and V_a are the axial ratio and viscosity of marker 'a' and $R_{xz(b)}$ and V_b are the axial ratio and viscosity of marker 'b'. Equation (2) is too simple to be universal and its linear form suggests the first approximation to a more complicated law. Although equation (2) was derived from data from three different regions, in all cases rocks are metamorphosed to greenschist facies from $R_{xz} \leq 3.2$ for quartz grains.

From equation (2) it follows that the quartz–pelitic schists viscosity ratio is about 3.5 (data from Norris & Bishop 1990, table 2). Based on Gay's (1968) theory, Norris & Bishop (1990) estimated the quartz–pelitic schists viscosity ratio to be somewhat higher (4–10) but, taking into the account abundance of approximations and suppositions in the theory and calculations, the similarity of the obtained results may be considered satisfactory.

According to equation (2) quartz–chert and quartz–pelitic schists viscosity ratios are similar and equal to 3.2 and 3.5, respectively. As pelitic schists make up a considerable proportion of the rocks (partly including

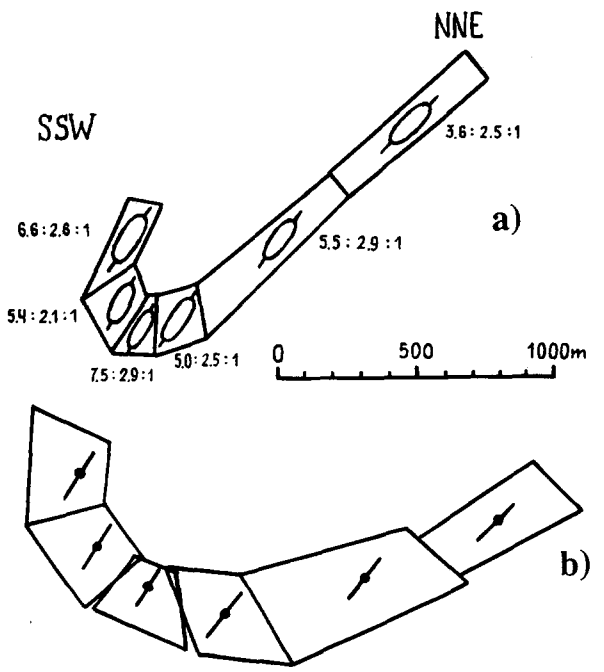

Fig. 11. Strain removal in a syncline near the CTT (the Usunakhmatian sheet). Location is shown in Fig. 10(c). Cross-section is YZ plane. (a) Present shape of fold and strain state. $X:Y:Z$ ratios are shown. (b) Shape of fold after strain removing. Increase in area is due to unplane strain (X axis is normal to cross-section plane).

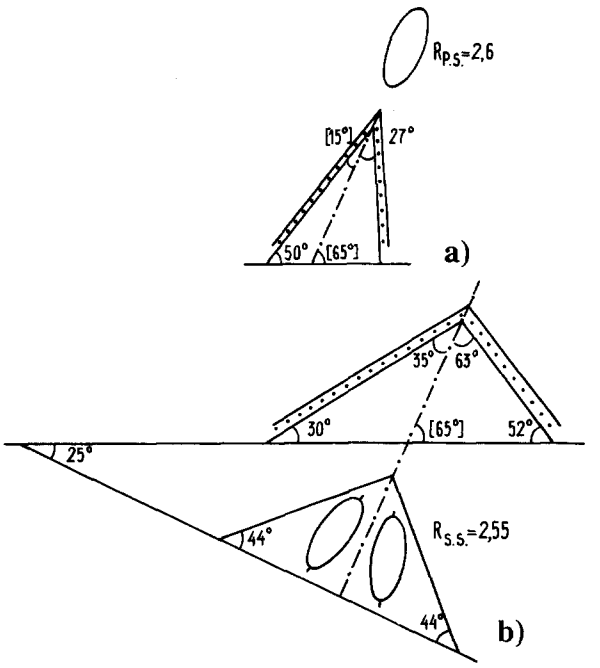

Fig. 12. Development of the Usunakhmatian sheet fold structures. Values of angles taken from Fig. 3(a), S_0 and S_2 are in brackets; other angles are calculated according to the Appendix. Dash–dot line is parallel to traces of cleavage and axial plane but not bisector of interlimb angle. (a) Present shape of average fold (after action of pure shear superimposed on previous fold). R_{yz} of pure shear strain ellipsoid (R_{ps}) is the mean value of the Usunakhmatian sheet (2.6). X axis of this ellipsoid is normal to plane of the section. (b) Shape of average fold before action of pure shear. Formation of the fold is connected with simple shear parallel to axial plane. R_{xz} of simple shear strain ellipsoid (R_{ss}) is 2.55. Y axis of this ellipsoid is normal to plane of the section.

the matrix of conglomerates) in the Usunakhmatian sheet, the similarity of viscosity ratios implies that the calculated strain from cherts is a fairly realistic evaluation of the bulk strain.

Type and history of strain

The restoration of rocks to their pre-deformation state by the strain reversal method of Woodward *et al.* (1986) was used to investigate the type of history of strain. The results are shown in Fig. 11. As it is seen from the comparison of Figs. 11(a) & (b), after the strain removal, a fold structure is still preserved with an interlimb angle of about 50° and with a southern limb which is vertical to overturned. This means that before the observed strain (calculated by the R_f/ϕ method) was imposed the rocks had already been subjected to some earlier strain. Similar results were obtained by Gray & Willman (1991) in the Ballarat Slate Belt, where the earlier strain was considered to be the result of buckling.

The result of buckling and flexural-slip is the appearance of folds in which the shape and orientation of strain ellipsoid varies greatly in the limits of each layer (Ramsay 1967, pp. 391–401). However, in the Usunachmatian sheet the shape and orientation of axes of strain ellipsoid varies moderately or slightly. It means that the earlier strain of the Usunachmatian sheet was hardly connected with buckling. More likely is simple shear parallel to axial plane. As was discussed above (Fig. 2), the formation of cleavage slightly pre-dated folding and the earlier formed cleavage might assist the mechanism of simple shear. The X axis of the observed strain ellipsoid is subhorizontal and parallel to the fold axes, and the Z axis is normal or subnormal to cleavage planes (Fig. 7). There are no clear folds and faults caused by subhorizontal extension, and it seems that subhorizontal fold axis parallel extension is compensated by subnormal to cleavage plane shortening. Taking into account data from Fig. 8 this strain is considered to be of pure shear type with some flattening.

Let us consider the effect of a superposition of pure shear on axial plane parallel simple shear in an 'average' anticlinal fold. Figure 3(a) (S_0 and S_2) shows that the axial plane of average fold dips to the southwest at the angle of 65° and the angle between axial plane and gentle limb is 15°. Let us suppose the following: (1) the fold shape is chevron; (2) the XY plane of the pure shear strain ellipsoid coincides with the axial plane of the fold; (3) before shearing the layers were horizontal; (4) a subvertical section normal to the fold axis and coinciding with the YZ plane of the pure shear strain ellipsoid is considered. All the necessary mathematical formulas are given in the Appendix, and the results of strain superposition are shown in Fig. 12. The angle between the gentle limb and axial plane of fold before pure shear is 35°, and formation of the fold in Fig. 12(b) is caused by simple shear with axial ratio $R_{xz} = 2.55$. The YZ plane of the pure shear strain ellipsoid coincides with the XZ plane of the simple shear strain ellipsoid and the angle between the Y axis of the former and the X axis of the latter being 14°. This means that the angle between the X

axis of resulting strain ellipsoid (after the application of the pure shear to the simple shear strain ellipsoid) and the axial plane of the fold in the section under consideration is about 5°. As there is some volume loss and therefore the R_f/ϕ method underestimates the true strain (Onasch 1984), the angle is naturally even less than 5°. This result is in agreement with data on Fig. 7(b).

Using this model, the strain history can be described as follows. The earliest event was simple shear, oriented at some angle (from 40° near the CTT to 90° near the TFF) to the horizontal plane. The importance of simple shear in the formation of thrusts and thrust–fold structures was emphasized by Ramsay (1981), Dietrich (1989), Elison & Speed (1989), Paterson *et al.* (1989), Paterson & Wainger (1991) and Plotnikov (1991). At this stage the fold axes were parallel to the Y axis of the strain ellipsoid. The next stage was deformation of existing fold and thrusts structures by pure shear, but at that stage the fold axes were parallel to the X axis of the strain ellipsoid. The observations on pyrite crystals show that near the faults they have small pressure shadows filled by antitaxial fibres of quartz and there are no pressure shadows at some distance from faults. The formation of pressure shadows was the third stage of strain history.

D_1 structures have no clearly identified cleavage and, according to Reks & Gray (1982), R_{xz} of corresponding strain could not be more than 1.8. The measurements of strain were made in samples out of locally developed D_3 structures. The formation of the regionally spread simple shear structures (cleavage, thrusts and folds) began during the D_2 phase, and cleavage slightly pre-dates other structures (Fig. 2). Thus, the most part of the observed strain had accumulated during D_2 deformation and three stages of strain history discussed above are subdivisions (or substages) of D_2 deformation. They are: D_{2a}—simple shear, D_{2b}—pure shear and D_{2c}—fibre growth.

Orogen parallel extension

The orientation of the axis of extension (the finite X axis) parallel to strike of the orogen is typical of many fold and thrust belts, but is manifest to different degrees. This is typical for the inner parts of the N. American Cordillera (Ellis & Watkinson 1987, Evans 1988, McDonough & Simony 1989) and metamorphic belts of Japan (Toriumi 1985, Shimizu 1988), having a subordinate role in the Helvetic nappes (Dietrich 1989) and being local or absent in the Himalayas (Ellis & Watkinson 1987, Bossart *et al.* 1988, Jain & Anand 1988) and southeastern Australia (Gray & Willman 1991). There is a very distinct orogen-parallel extension in the Usunakhmatian sheet, where the stretching lineation and X axis are parallel to the fold axes.

The value of orogen-parallel extension in the Usunakhmatian sheet varies from 60% (in the locality with $X:Y:Z = 2.4:1.4:1$) up to 170% ($X:Y:Z = 7.5:2.9:1$) with a mean value near 120% (Khudoley in press). Such considerable magnitudes are usually explained by oblique tectonics (Ellis & Watkinson 1987, McDonough & Simony 1989), oroclinal bending of structures (Ries & Shackleton 1976), a change in the direction of overthrust shearing (Dietrich 1989) and rotation and reorientation of the X axis to the fold axes (Evans 1988). According to Srivastava & Engelder (1990) strike-parallel stretching is required to accommodate the lateral ramps in the Appalachian Valley and Ridges. Shimizu (1988) argues that strain patterns of the Sambagawa belt are in agreement with ideas that strain magnitude depends mostly on metamorphic temperature (Toriumi 1985) and oblate strain ellipsoids in lower grade metamorphic rocks transform to prolate strain ellipsoids in higher grade metamorphic rocks. Toriumi (1985) considers strike-parallel extension to be the result of simple shear during subduction and rolling fragments of an accretionary wedge. Lukjanov (1980), based on centrifuge modelling of tectonic processes, supports the ideas of tectonic delamination of the lithosphere and shows that at some level of the crust extension in the horizontal plane might take place as well as vertical flattening and rising temperature.

The observed extension in the Talassian Alatau could not be connected with oblique tectonics. Oblique movements may be related to D_3 (Fig. 4), but parallelism of the axes of extension and D_2 structures to the main fault of the region (the TFF) cannot be explained by oblique tectonics. Finally, in the Talassian Alatau extension (pure shear) was superimposed on already formed folds and thrusts (simple shear), whereas Ellis & Watkinson's (1987) model suggests the reverse sequence of events. Predominance of approximately plane strain and the absence of a typical divergent system of thrusts ('flower structure') near the main strike-slip fault (the TFF) makes transpression also an unfavourable mechanism (Sanderson & Marchini 1984). The straight form of the orogen excludes oroclinal bending and implies orthogonal contraction. D_3 deformation led to local reorientations only and was not intense enough to rotate X axes to fold axes in all of the Usunakhmatian sheet. Structural and mineralogical associations of rocks (Frolova 1982) argues for the importance of pressure rather than that of temperature. Plane strain and flattening observed in the Usunakhmatian sheet are typical for collision orogens and contradict Toriumi's (1985) model, which predicts an intense uniaxial extension type of strain. In spite of the presence of small ramps (Khudoley & Semiletkin in press), there is no data about their widespread occurrence and role in the fold–thrust structure of the Talassian Alatau. The models of Lukjanov (1980) and Dietrich (1989) seem to be more acceptable. Systematic decrease from the TFF to the CTT of the dips of the imbricate thrusts, axial planes of folds, cleavage and XY planes is typical for the Usunakhmatian sheet and similar to that observed in the Helvetic nappes (figs. 3–5 in Ramsay 1981), although there are no proved large recumbent folds in the former. In this case, the TFF occupies the same structural position as the root zone of the Helvetic nappes, despite an absence of structural units analogous with the Penninic nappes in

the Talassian Alatau. Simple shear was important in both regions, and the change in direction of overthrust shear which was responsible for the fold-axis parallel extension in the Helvetic nappes (see fig. 28 in Dietrich 1989) might be one of the mechanisms of fold-axis parallel extension in the Usunakhmatian sheet. As has been mentioned above, the Kumishtagian and, partly, the Talassian sheets (Fig. 1c) were overthrusted on to the Usunakhmatian sheet before D_2 deformation of the latter. Rocks of the Usunakhmatian sheet were submerged to considerable depth reaching assumed levels where oblate strain ellipsoid become more prolate (Shimizu 1988) and conditions of horizontal extension were realized (Lukjanov 1980). The submerging of the Usunakhmatian sheet to considerable depth before D_2 deformation could be the second mechanism of orogen-parallel extension.

CONCLUSIONS

Three phases of deformation were involved in the development of the structures in the Usunakhmatian sheet. Strain measurements were made from samples taken from locally developed D_3 structures, and R_{xz} corresponding to the strain of the D_1 phase could not be more than 1.8. The most part of measured strain (with R_{xz} up to 7.5) was due to penetrative D_2 deformation. There are the following three substages: D_{2a}—simple shear, D_{2b}—pure shear and D_{2c}—fibre growth.

R_{xz} values determined from quartz and chert grains (using the R_f/ϕ method) have a linear relationship. Equation (2) is supported by data of Lisle *et al.* (1983) and Norris & Bishop (1990) and implies a rather simple correlation between axial and viscosity ratios. Equation (2) allows the data set to be enhanced and comparison of the strain of markers with different viscosity in greenschists.

The mean strain of the Usunakhmatian sheet is approximately plane strain with some flattening. The X axis is parallel to the fold axes and the strike of the orogen. The corresponding mean value of orogen-parallel extension is about 120% and might be caused by a change in the direction of overthrust simple shear (Dietrich 1989) or burial to some depth, where environments of horizontal extension are important (Lukjanov 1980).

Acknowledgements—Two reviewers, S. R. Paterson and C. M. Onasch, and R. J. Lisle made very helpful comments and corrections to the text style. Some problems of regional geology of the Talassian Alatau were discussed with S. A. Semiletkin. E. P. Kulkov helped to translate the text into English. N. P. Voevodina drafted the illustrations.

REFERENCES

Afonichev, N. A. & Vlasov, N. G. (editors) 1984. *Geologic Map of the Kazakhstan and Middle Asia*, scale 1:1 500 000. Appendices. VSEGEI Press, Leningrad (in Russian).

Becker, A. Y. 1987. On the relations between tectonic structures of the Usunakhmatian and Karagainian blocks of the Talasso-Karatausian structural-formation zone (Northern Tien-Shan). In: *Kaledonides of Tien-Shan* (edited by Korolev, V. G.). Ilim, Frunze, 21–36 (in Russian).

Becker, A. Y., Makarov, V. A. & Razboinikov, A. G. 1988. New data on the stratigraphy of Karagainian Group of the Talassian Ala-Too (Northern Tien-Shan). In: *Precambrian and Lower Paleozoic of Tien-Shan* (edited by Kiselev, V. V.). Ilim, Frunze, 100–126 (in Russian).

Beloussov, V. V. 1975. *Elements of Geotectonics*. Nedra, Moscow (in Russian).

Beloussov, V. V. 1985. *Elements of Structural Geology*. Nedra, Moscow (in Russian).

Borradaile, G. J., Bayly, M. B. & Powell, C. McA. (editors) 1982. *Atlas of Deformational and Metamorphic Rock Fabrics*. Springer, Berlin.

Bosart, P., Dietrich, D., Greco, A., Ottiger, R. & Ramsay, J. G. 1988. The tectonic structure of the Hazara–Kashmir syntaxis, Southern Himalayas, Pakistan. *Tectonics* **7**, 273–297.

Boyer, S. E. & Elliott, D. 1982. Thrust systems. *Bull. Am. Ass. Petrol. Geol.* **66**, 1196–1230.

Burtman, V. S. 1964. *Talaso–Ferganian Strike-slip Fault (Tien-Shan)*. Nauka, Moscow (in Russian).

Cashman, S. M. 1988. Finite-strain patterns of Nevadan deformation, western Klamath Mountains, California. *Geology* **16**, 839–843.

De Paor, D. G. 1988. R_f/ϕ_f strain analysis using an orientation net. *J. Struct. Geol.* **10**, 323–333.

Dietrich, D. 1989. Fold axis parallel extension in an arcuate fold and thrust belt: the case of the Helvetic nappes. *Tectonophysics* **170**, 183–211.

Dunne, W. M., Onasch, C. M. & Williams, R. I. 1990. The problem of strain-marker centers and the Fry method. *J. Struct. Geol.* **12**, 933–938.

Elison, M. W. & Speed, R. C. 1989. Structural development during flisch basin collapse: the Fencemaker allochthon, East Range, Nevada. *J. Struct. Geol.* **11**, 523–538.

Ellis, M. A. & Watkinson, A. J. 1987. Orogen-parallel extension and oblique tectonics: the relation between stretching lineations and relative plate motions. *Geology* **15**, 1022–1026.

Evans, J. G. 1988. Deformation in the Stensgar Mountain Quadrangle, Stevens County, Washington. *Bull. U.S. geol. Surv.* **1820**.

Frolova, N. S. 1982. Influence of metamorphism on deformation properties of rocks (example from the Talassian Alatau). *Geotectonics* **N4**, 18–24 (in Russian).

Fry, N. 1979. Random point distribution and strain measurement in rocks. *Tectonophysics* **60**, 89–105.

Gay, N. C. 1968. Pure shear and simple shear deformation of inhomogeneous viscous fluids. 1. Theory. *Tectonophysics* **5**, 211–234.

Ghosh, S. K. 1982. The problem of shearing along axial plane foliations. *J. Struct. Geol.* **4**, 63–67.

Goncharov, M. A. 1979. *Density Inversion in the Earth's Crust and Folding*. Nauka, Moscow (in Russian).

Gray, D. R. & Willman, C. E. 1991. Thrust-related strain gradients and thrusting mechanisms in a chevron-folded sequence, southeastern Australia. *J. Struct. Geol.* **13**, 691–710.

Jain, A. K. & Anand, A. 1988. Deformational and strain patterns of an intracontinental collision ductile shear zone—an example from the Higher Garhwal Himalaya. *J. Struct. Geol.* **7**, 717–734.

Khudoley, A. K. In press. Quantitative estimation of strain in the Talaso–Ferganian Fault zone. In: *Tectonophysic Aspects of Faulting in Lithosphere* (edited by Sherman, S. I.) (in Russian).

Khudoley, A. K. & Semiletkin, S. A. In press. Morphology and evolution of fold and fault structures of the Talassian Alatau (Northern Tien-Shan). *Geotectonics* (in Russian).

Kiselev, V. V. & Korolev, V. G. 1981. *Paleotectonics of the Tien-Shan Precambrian and Lower Paleozoics*. Ilim, Frunze (in Russian).

Kiselev, V. V., Apaiarov, F. H., Komarevzev, V. T. & Ziganok, A. N. 1986. New data on uran-plumbum ages of stratificated rocks of the Tien-Shan. In: *Methods of Isotopic Geology and Geochronologic Scale* (edited by Schukoliukov, Y. A. & Bibikova, E. V.). Nauka, Moscow, 215–225 (in Russian).

Korolev, V. G., Kiselev, V. V. & Maksumova, R. A. 1983. Basic patterns of the North and Middle Tien-Shan Paleozoic tectonics in Kirgizian SSR. In: *Tectonics of the Tien-Shan and Pamir* (edited by Gubin, I. E. & Zakharov, S. A.). Nauka, Moscow, 55–60 (in Russian).

Lisle, R. J. 1977. Estimation of the tectonic strain ratio from the mean shape of deformed elliptical markers. *Geologie Mijnb.* **56**, 140–144.

Lisle, R. J. 1985. *Geological Strain Analysis: A Manual for the R_f/ϕ Technique*. Pergamon Press, Oxford.

Lisle, R. J., Rondeel, H. E., Doorn, D., Brugge, J. & Van de Gaage, P. 1983. Estimation of viscosity contrast and finite strain from deformed elliptical inclusions. *J. Struct. Geol.* **5**, 603–609.
Lukjanov, A. V. 1980. Ductile deformations and tectonic flow of rocks in lithosphere. In: *Tectonic Delaminations of Lithosphere* (edited by Peive, A. V.). Nauka, Moskow, 105–146 (in Russian).
McDonough, M. R. & Simony, P. S. 1989. Valemount strain zone: a dextral oblique-slip thrust system linking the Rocky Mountain and Omineca belts of the southeastern Cordillera. *Geology* **17**, 237–240.
Milton, N. J. & Williams, G. D. 1981. The strain profile above a major thrust fault, Finmark, N. Norway. In: *Thrust and Nappe Tectonics* (edited by McClay, K. & Price, N. J.). *Spec. Publs geol. Soc. Lond.* **9**, 235–239.
Norris, R. J. & Bishop, D. G. 1990. Deformed conglomerates and textural zones in the Otago Schists, South Island, New Zealand. *Tectonophysics* **174**, 331–349.
Onasch, C. M. 1984. Application of the R_f/ϕ technique to elliptical markers deformed by pressure-solution. *Tectonophysics* **110**, 157–164.
Onasch, C. M. 1986. Ability of the Fry method to characterize pressure–solution deformation. *Tectonophysics* **122**, 187–193.
Paterson, S. R. 1983. A comparison of methods used in measuring finite strain from ellipsoidal objects. *J. Struct. Geol.* **5**, 611–618.
Paterson, S. R., Tobisch, O. T. & Bhattacharyya, T. 1989. Regional, structural and strain analyses of terranes in the Western Metamorphic Belt, Central Sierra Nevada, California. *J. Struct. Geol.* **11**, 255–273.
Paterson, S. R. & Wainger, L. 1991. Strains and structures associated with a terrane bounding stretching fault: the Melones fault zone, central Sierra Nevada, California. *Tectonophysics* **194**, 69–90.
Plotnikov, L. M. 1991. *Shear Structures in Layered Geological Bodies*. Nedra, Leningrad (in Russian).
Pomazkov, K. D., Eliutin, D. N., Knauf, V. L. & Korolev, V. G. 1972. *Geology of Kirgizian SSR (Geology of USSR, Volume XXV, Book* 2). Nedra, Moscow (in Russian).
Rajlich, P. 1990. Strain and tectonic styles related to Variscian transpression and transtension in Moravo–Silesian Culmian basin, Bohemian Massif, Czechoslovakia. *Tectonophysics* **174**, 351–367.
Ramsay, J. G. 1967. *Folding and Fracturing of Rocks*. McGraw-Hill, New York.
Ramsay, J. G. 1981. Tectonics of the Helvetic nappes. In: *Thrust and Nappe Tectonics* (edited by McClay, K. & Price, N. J.). *Spec. Publs geol. Soc. Lond.* **9**, 293–309.
Ramsay, J. G. & Huber, M. I. 1983. *The Techniques of Modern Structural Geology, Volume* 1: *Strain Analysis*. Academic Press, London.
Reks, I. J. & Gray, D. R. 1982. Pencil structure and strain in weakly deformed mudstone and siltstone. *J. Struct. Geol.* **4**, 161–176.
Ries, A. C. & Shackleton, R. M. 1976. Patterns of strain variations in arcuate fold belts. *Phil. Trans. R. Soc. Lond.* **A283**, 281–288.
Sanderson, D. J. & Marchini, W. R. D. 1984. Transpression. *J. Struct. Geol.* **6**, 449–458.
Shimizu, I. 1988. Ductile deformation in the low-grade part of the Sambagawa metamorphic belt in the northern Kanto Mountains, central Japan. *J. geol. Soc. Japan* **94**, 609–628.
Srivastava, D. C. & Engelder, T. 1990. Crack-propagation sequence and pore-fluid conditions during fault-bend folding in the Appalachian Valley and Ridge, central Pennsylvania. *Bull. geol. Soc. Am.* **102**, 116–128.
Suvorov, A. I. 1968. *Regularites in the Structure and Development of Deep Faults*. Nauka, Moscow (in Russian).
Sylvester, A. C. 1988. Strike-slip faults. *Bull. geol. Soc. Am.* **100**, 1666–1703.
Toriumi, M. 1985. Two types of ductile deformation/regional metamorphic belt. *Tectonophysics* **113**, 307–326.
Treagus, S. H. 1988. Strain refraction in layered system. *J. Struct. Geol.* **10**, 517–527.
Uemura, T. & Mizutani S. (editors) 1984. *Geological Structures*. John Wiley and Sons, Chichester.
Woodward, N., Gray, D. & Spears, D. 1986. Including strain in balanced cross-sections. *J. Struct. Geol.* **8**, 313–324.

APPENDIX

The mathematical relations between different angles in the folds of axial plane parallel simple shear and the subsequent pure shear are considered below. To simplify the calculations it is assumed that the fold has a chevron shape and the section is normal to fold axes (Fig. A1). In the cases when shearing direction is not normal to horizontal layers the axial plane and cleavage are parallel to each other, but they do not coincide with the bisector of the interlimb fold angle. From stereonet analyses (Fig. 3a, S_0 and S_2) we know the angles b and e. It is necessary to calculate all the others. Evidently, $\alpha = 90 - e$ and $a = e - b$. Let us designate A, B, C for the sides of the triangles lying opposite the angles a, b, c. As $B = C$, from the sine rule it follows that:

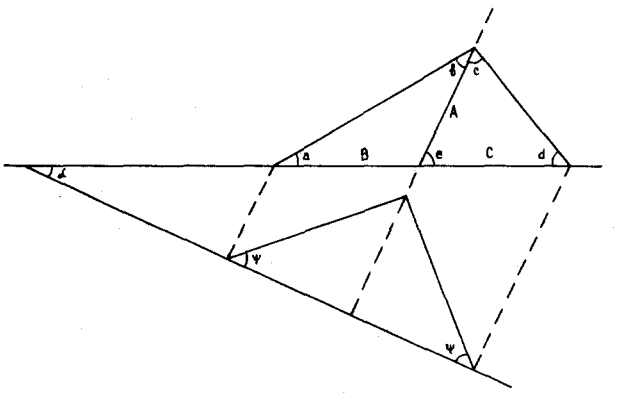

Fig. A1. Definition of angular and linear elements in fold formed by simple shear parallel to axial plane when direction of shearing is not normal to horizontal layering.

$$\frac{\sin d}{\sin c} = \frac{A}{B} = \frac{\sin a}{\sin b} = k \quad \text{or} \quad \sin d = k \sin c$$

$$\gamma = \tan \psi = \frac{A}{B \cos \alpha} = \frac{k}{\cos \alpha},$$

where γ is shear strain.

Let us consider the value $m = -\sin \alpha$:

$$m = -\sin \alpha = \cos(\alpha + 90) = \cos[180 - (90 - \alpha)]$$
$$= \cos(c + d) = \cos c \cdot \cos d - \sin c \cdot \sin d$$
$$= \sqrt{1 - \sin^2 c} \cdot \sqrt{1 - k^2 \sin^2 c} - k \sin^2 c.$$

Raise to the second power both parts of the last equation:

$$(m + k \sin^2 c)^2 = (1 - \sin^2 c)(1 - k^2 \sin^2 c).$$

Transforming this, we get:

$$\sin c = \left(\frac{1 - m^2}{2mk + k^2 + 1}\right)^{1/2}.$$

This equation allows us to determine angles α, γ, a, c and d from given angles b and e. The shape and orientation of strain ellipsoid formed by simple shear with the shear strain γ is determined as follows:

$$R_s = \frac{(\gamma^2 + 2)\sqrt{4 + \gamma^2} + \gamma(\gamma^2 + 4)}{(\gamma^2 + 2)\sqrt{4 + \gamma^2} - \gamma(\gamma^2 + 4)}$$

(after Ramsay and Huber 1983, p. 30),

$$\tan \psi = 2 \cot 2\delta \qquad \text{(Ramsay and Huber 1983)}$$

where δ is the angle between the long axis of strain ellipsoid and the shear direction.

Next, consider deformation of the anticlinal fold on Fig. A1 by pure shear. The deviation from the plane strain will influence the fold amplitude and thickness of layers but not the fold shape. According to Harker's formula $\tan \theta_1 = R_s \tan \phi_1$, where θ_1 is the angle between a line and the short axis of strain ellipsis before the application of strain with strain ratio R_s and ϕ_1 is the same angle after the application of strain. In the example under consideration (Fig. A1) Harker's formula has the following form:

$$\tan(a + \alpha) = R_s \tan(a' + \alpha) \quad \text{and} \quad \tan(d - \alpha) = R_s \tan(d' - \alpha),$$

where a' and d' are the angles after the application of pure shear and α and e remain constant. The task of determining the orientation and the shape of resulting strain ellipse is the same task as deforming elliptical objects by pure shear. According to Ramsay (1967, pp. 205–209) and Lisle (1985, p. 3) the shape and orientation of resulting strain ellipse is defined as (Fig. A2):

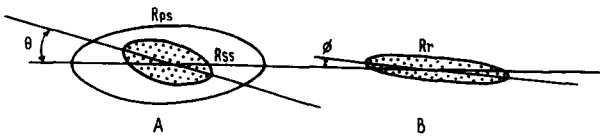

Fig. A2. Application of pure shear (R_{ps}) to elliptical object formed by simple shear (R_{ss}). (b) Shape and orientation of resulting strain ellipse. In the example under consideration: $R_{ps} = 2.6$, $R_{ss} = 2.5$, $\phi = 14°$, $R_r = 6.4$ and $\theta = 5°$.

$$\tan 2\phi = \frac{2R_{ps}(R_{ss}^2 - 1)\sin 2\theta}{(R_{ss}^2 + 1)(R_{ps}^2 - 1) + (R_{ss}^2 - 1)(R_{ps}^2 + 1)\cos 2\theta}$$

$$R_r = \left[\frac{\tan^2\phi(1 + R_{ss}^2\tan^2\theta) - R_{ps}^2(\tan^2\theta + R_{ss}^2)}{R_{ps}^2\tan^2\phi\,(\tan^2\theta + R_{ss}^2) - (1 + R_{ss}^2\tan^2\theta)}\right]^{1/2},$$

where θ and ϕ are the angles between the long axis of pure shear strain ellipse (coincides with direction of cleavage dip) and long axes of strain ellipses of simple shear and the resulting one, and R_{ps}, R_{ss} and R_r are the strain ratios of pure shear, simple shear and resulting strain ellipses, respectively.